Circulation Research
Journal of the American Heart Association

Alternative Splicing of Ryanodine Receptors Modulates Cardiomyocyte Ca2+ Signaling and Susceptibility to Apoptosis

Christopher H. George, Sarah A. Rogers, Benedicte M.A. Bertrand, Richard E.A. Tunwell, N. Lowri Thomas, Derek S. Steele, Eryl V. Cox, Christopher Pepper, Carolyn J. Hazeel, William C. Claycomb and F. Anthony Lai

Circ Res. 2007;100:874-883; originally published online February 22, 2007;
doi: 10.1161/01.RES.0000260804.77807.cf
Circulation Research is published by the American Heart Association, 7272 Greenville Avenue, Dallas, TX 75231

Print ISSN: 0009-7330. Online ISSN: 1524-4571

Alternative Splicing of Ryanodine Receptors Modulates Cardiomyocyte Ca^{2+} Signaling and Susceptibility to Apoptosis

Christopher H. George, Sarah A. Rogers, Benedicte M.A. Bertrand, Richard E.A. Tunwell, N. Lowri Thomas, Derek S. Steele, Eryl V. Cox, Christopher Pepper, Carolyn J. Hazeel, William C. Claycomb, F. Anthony Lai

Abstract—Ca^{2+} release via type 2 ryanodine receptors (RyR2) regulates cardiac function. Molecular cloning of human RyR2 identified 2 alternatively spliced variants, comprising 30- and 24-bp sequence insertions; yet their role in shaping cardiomyocyte Ca^{2+} signaling and cell phenotype is unknown. We profiled the developmental regulation and the tissue and species specificity of these variants and showed that their recombinant expression in HL-1 cardiomyocytes profoundly modulated nuclear and cytoplasmic Ca^{2+} release. All splice variants localized to the sarcoplasmic reticulum, perinuclear Golgi apparatus, and to finger-like invaginations of the nuclear envelope (nucleoplasmic reticulum). Strikingly, the 24-bp splice insertion that was present at low levels in embryonic and adult hearts was essential for targeting RyR2 to an intranuclear Golgi apparatus and promoted the intracellular segregation of this variant. The amplitude variability of nuclear and cytoplasmic Ca^{2+} fluxes were reduced in nonstimulated cardiomyocytes expressing both 30- and 24-bp splice variants and were associated with lower basal levels of apoptosis. Expression of RyR2 containing the 24-bp insertion also suppressed intracellular Ca^{2+} fluxes following prolonged caffeine exposure (1 mmol/L, 16 hours) that protected cells from apoptosis. The antiapoptotic effects of this variant were linked to increased levels of Bcl-2 phosphorylation. In contrast, RyR2 containing the 30-bp insertion, which was abundant in human embryonic heart but was decreased during cardiac development, did not protect cardiomyocytes from caffeine-evoked apoptosis. Thus, we provide the first evidence that RyR2 splice variants exquisitely modulate intracellular Ca^{2+} signaling and are key determinants of cardiomyocyte apoptotic susceptibility. (***Circ Res*****. 2007;100:874-883.)**

Key Words: ryanodine receptor ■ Ca^{2+} ■ alternative splicing ■ cardiomyocyte ■ apoptosis

Alternative splicing of pre-mRNA transcripts is a powerful mechanism to generate remarkable protein diversity from single genes and is a prevalent feature of human gene processing. The plasticity of multiprotein signaling networks is greatly augmented by the regulated expression of distinct protein variants that expand the cellular signaling repertoire. The spatiotemporal encoding of intracellular Ca^{2+} signaling is exquisitely modulated by alternative splicing of phosphodiesterases, plasma membrane Ca^{2+}-ATPases, Trp channels, L-type Ca^{2+} channels, inositol 1,4,5-trisphosphate receptors, sodium calcium exchangers, sarcoplasmic reticulum (SR)/endoplasmic reticulum (ER) Ca^{2+}-ATPases (SERCAs), and Ca^{2+}/CaM-dependent protein kinase II, according to cell type and developmental stage, and in response to neurohumoral stimuli, mechanical forces, and cellular stress.

Ryanodine receptors (RyRs) are enormous tetrameric channels that transduce an array of cellular inputs to elicit synchronous Ca^{2+} release from the SR to initiate muscle contraction and regulate numerous processes.[1,2] The functional diversity of RyRs is reflected in the structural organization of the polypeptide as a series of contiguous functional domains.[3] The human genes encoding RyR isoforms are some of the largest and most complex in the genome, comprising >100 exons. To date, 13 distinct splice variants have been identified in RyR isoforms cloned from mammalian and insect species (see Figure 1A and the online data supplement [Table I] at http://circres.ahajournals.org), reflecting the evolutionary importance of alternative splicing in RyR2 modulation. Ca^{2+} release channels formed from RyR1 subunits containing a devel-

Original received August 15, 2006; resubmission received January 11, 2007; revised resubmission received January 31, 2007; accepted February 8, 2007.

From the Department of Cardiology (C.H.G., S.A.R., B.M.A.B., N.L.T., E.V.C., C.J.H., F.A.L.), Wales Heart Research Institute, Cardiff University, UK; Department of Physiology (R.E.A.T.), University College London, UK; Institute of Membrane and Systems Biology (D.S.S.), University of Leeds, UK; Department of Haematology (C.P.), Cardiff University School of Medicine, UK; and Department of Biochemistry (W.C.C.), Louisiana State University, New Orleans.

Correspondence to Dr Christopher H. George, Department of Cardiology, Wales Heart Research Institute, School of Medicine, Cardiff University, Heath Park, Cardiff CF14 4XN, UK. E-mail georgech@cf.ac.uk

Circulation Research **is available at http://circres.ahajournals.org** **DOI: 10.1161/01.RES.0000260804.77807.cf**

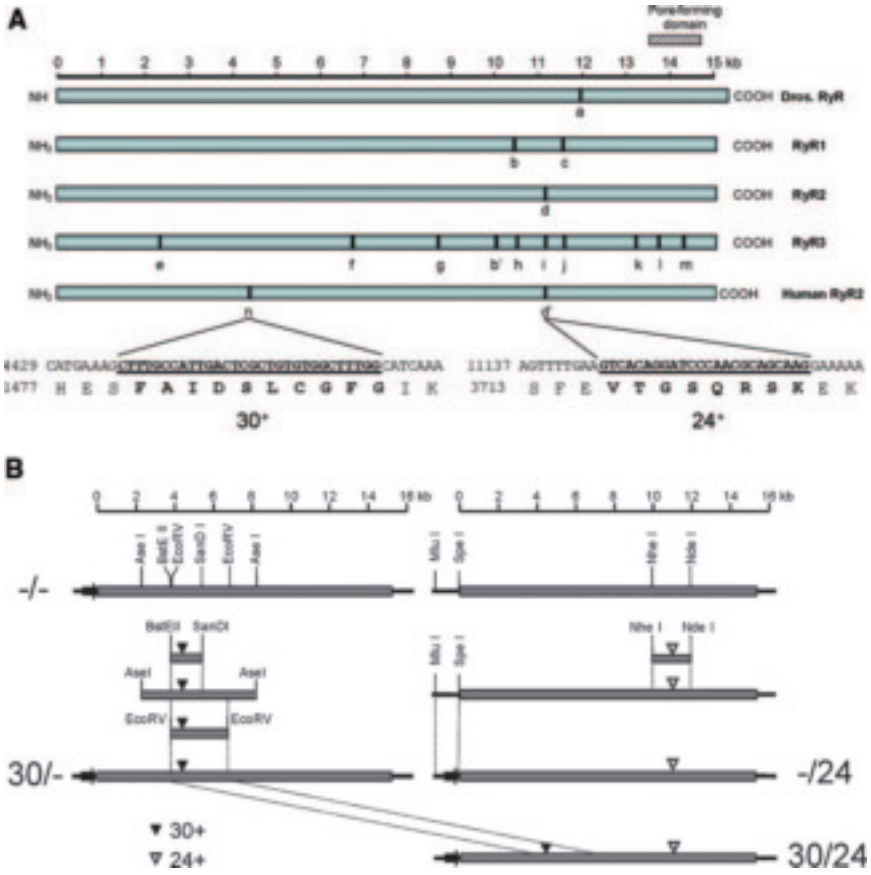

Figure 1. Construction of human RyR2 containing 30-bp and 24-bp splice insertions. A, Thirteen RyR splice variants have been identified in human, rabbit, mouse, mink, dog, and *Drosophila* (see supplemental Table I). RyR1 and RyR3 variants b and b′, respectively, are equivalent. The 24-bp insertion in human RyR2 (d′) is identical to that in the rabbit and canine RyR2 sequences. B, Construction of eGFP-tagged RyR2 containing 30-bp ($RyR2^{30/-}$), 24-bp ($RyR2^{-/24}$), or both ($RyR2^{30/24}$) splice insertions. 224 indicates eGFP.

opmentally regulated, disease-linked splice insertion exhibited distinct Ca^{2+}-releasing profiles in skeletal myotubes,[4] and a smooth-muscle–specific deletion in RyR3 that did not form functional homotetrameric channels, inhibited Ca^{2+} release when expressed in heteromeric combination with RyR isoforms that lacked insertions[5,6] (Figure 1A and supplemental Table I, variants b and k, respectively).

Two alternatively spliced variants of the human cardiac RyR channel (RyR2) corresponding to a 30-bp insertion (encoding FAIDSLCGFG) and a 24-bp insertion (encoding VTGSQRSK) (variants n and d′, respectively; Figure 1A and supplemental Table I) have been identified.[7] However, their roles in cardiac development and cell signaling have remained a mystery. Here, we present the first functional characterization of human RyR2 splice variants and show that cellular architecture and Ca^{2+} signaling are profoundly modulated following their expression in HL-1 cardiomyocytes. Our data highlight an important role for the 24-bp insertion in protecting cardiomyocytes from stimulation-induced apoptosis and thus identify RyR2 alternative splicing as a key determinant of cardiomyocyte susceptibility to apoptosis. Furthermore, we show that the expression profiles of RyR2 splice variants exhibits distinct species-, tissue-, and developmentally specific regulation, and we evaluate the implications of our findings in the context of cardiac development and future therapeutic approaches to cardiac disease.

Materials and Methods

Construction, Expression, and Detection of Human RyR2 Splice Variants

The recombinant human RyR2 routinely expressed in our laboratory lacks the 30-bp and 24-bp splice insertions and is subsequently referred to as $RyR2^{-/-}$. The construction of enhanced green fluorescence protein (eGFP)-tagged RyR2 containing the 30-bp exon ($RyR2^{30/-}$), 24-bp exon ($RyR2^{-/24}$), or both insertions ($RyR2^{30/24}$) is shown in Figure 1B and the online data supplement. N-terminal tagging of $RyR2^{-/-}$ with *Discosoma sp* red fluorescent protein (DsRed) was performed as described.[8]

HL-1 cardiomyocytes were cultured and transfected with recombinant RyR2 as described.[8] Cells expressing eGFP-tagged RyR2 were selected by G418-sulfate resistance (500 μg/mL) and were isolated using fluorescent-activated cell sorting (FACS) based on eGFP intensity.[9] FACS-enriched cells were used as the background for DsRed-tagged $RyR2^{-/-}$ expression. The intracellular localization of recombinant RyR2 was visualized using eGFP or DsRed fluorescence,[10] and pAb129 was used for immunodetection of endogenous and recombinant RyR2.[8] Antibodies to eGFP, DsRed, calreticulin (an ER marker), and a Golgi matrix protein (GM130) are described in the online data supplement. Profiling the species, tissue, and developmental aspects of RyR2 splice variant expression are described in the online data supplement.

Ca^{2+} Imaging and Signal/Noise Analysis

Ca^{2+} release triggered by the acute addition of caffeine (10 mmol/L) or following tonic RyR2 activation by prolonged exposure to caffeine (1 mmol/L, 16 hours) was determined in single fluo3-loaded cells using confocal microscopy (RS2, Leica Microsystems).[11] Analysis of the amplitude and temporal variability in resting and caffeine-activated Ca^{2+} fluxes in nuclear and cytoplasmic regions

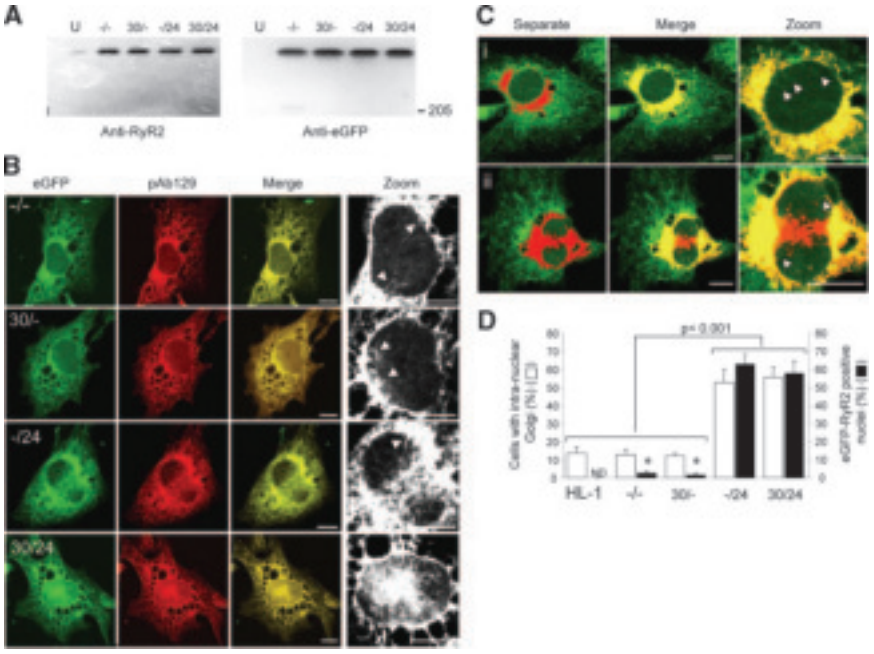

Figure 2. Intracellular segregation of RyR2 splice variants in HL-1 cardiomyocytes. A, Immunoblot analysis of total cell lysates (200 μg) obtained from FACS-enriched HL-1 cardiomyocytes expressing RyR2 splice variants or from nontransfected control cells (U). We determined equivalent relative expression of $RyR2^{-/-}$, 3.84±0.28; $RyR2^{30/-}$, 4.31±0.47; $RyR2^{-/24}$, 3.61±0.52; $RyR2^{30/24}$,4.07±0.61 when compared with endogenous RyR2 expression assigned 1.0, based on densitometric analysis of 3 separate FACS enrichments. B, The intracellular localization of RyR2 splice variants was visualized using endogenous eGFP fluorescence (green) or pAb129 immunodetection (red). Coincident signals appear yellow (Merge). Bar represents 10 μm. C, HL-1 cardiomyocytes stained with antibodies against ER (calreticulin, green) and GA (GM130, red) demonstrated 2 distinct patterns of GA architecture (i and ii), comprising 88.7% and 11.3% of the total cell population, respectively. Coincident pixels appear yellow (Merge). Arrowheads indicate NR that is distinct from the transnuclear distribution characteristic of INGA (ii). Bar represents 10 μm. D, The presence of INGA was determined by GM130 staining (white bars), and the localization of RyR2 splice variants was visualized by eGFP fluorescence (black bars). Data are given as means±SEM (n=4, >300 cells per experiment). *$P<0.005$ within grouping. ND indicates not determined.

was performed as described (see the expanded Materials and Methods section in the online data supplement).[9,11]

Determination of Cell Viability and Mode of Cell Death

Cell viability, and the extent of apoptosis versus necrosis (where "necrosis" is used to describe a mode of cell death that is distinct from apoptosis[12]), was determined.[11]

Transcriptional and Protein Expression Analysis of Bcl-2

The levels of Bcl-2 mRNA transcripts in untreated cells or following their prolonged exposure to caffeine (1 mmol/L, 16 hours) were determined using quantitative PCR. The expression levels and phosphorylation status of the endogenous Bcl-2 protein was determined by immunoblotting. Detailed methods are included in the online data supplement.

Results

Alternative Splicing Determines the Cellular Localization of RyR2

Recombinant eGFP-tagged RyR2 splice variants were overexpressed to equivalent levels in FACS-enriched HL-1 cardiomyocytes (Figure 2A). Coincident fluorescent signals from N-terminal eGFP and C-terminal pAb129 immunodetection confirmed the expression of full-length recombinant RyR2. All RyR2 splice variants were localized to an extensive lattice-like network consistent with ER, the nucleoplasmic reticulum (NR) (finger-like invaginations of the nuclear envelope [NE]),[13,14] and a perinuclear accumulation characteristic of the Golgi apparatus (GA) (Figure 2B). The localization of recombinant RyR2 to these compartments was indistinguishable for the cellular distribution of endogenous RyR2 (supplemental Figure I). The localization of RyR2 splice variants to these compartments was confirmed by antibody mapping of ER and GA (using compartment-specific markers calreticulin and GM130, respectively), although the extensive colocalization of GA and ER in the perinuclear region of HL-1 cardiomyocytes precluded the unambiguous identification of all RyR2 splice variants to perinuclear GA (Figure 2Ci). However, we identified a subpopulation of HL-1 cells (comprising ≈11% of the total cell population) that exhibited a remarkably distinct intranuclear GA organization (INGA) that accounted for 12.1±4.3% of the total cellular GA content (Figure 2Cii). The different GA architecture in HL-1 populations did not affect cellular morphology (Figure 3), size (760±92 μm^2 versus 830±118 μm^2), viability (89±10% versus 86±15%), or nuclear size (132±24 μm^2 versus 153±27 μm^2), where data refer to INGA-negative versus INGA-positive HL-1 populations, respectively.

Recombinant RyR2 containing the 24-bp insertion ($RyR2^{-/24}$ and $RyR2^{30/24}$) exhibited striking intranuclear distribution, localizing to fibrillar-like structures that were distinct from the NR, yet were indistinguishable from the INGA morphology identified using anti-GA antibodies (Figure 2B and 2C). Analysis of fluorescent signal intensity revealed that INGA-localized $RyR2^{-/+}$ and $RyR2^{+/+}$ accounted for 9.3±3.6% and 11.4±4.6% of the total cellular content of recombinant RyR2, respectively, entirely consistent with the proportion of cellular GA that comprises INGA (11.3%). Costaining of GA and RyR2 splice variants revealed that INGA localization was restricted to $RyR2^{-/24}$ and $RyR2^{30/24}$ and that the number INGA-positive cells was increased by more than 4-fold following $RyR2^{-/24}$ and $RyR2^{30/24}$ expression (Figure 2D). Analysis of discrete FACS-isolated cell populations ex-

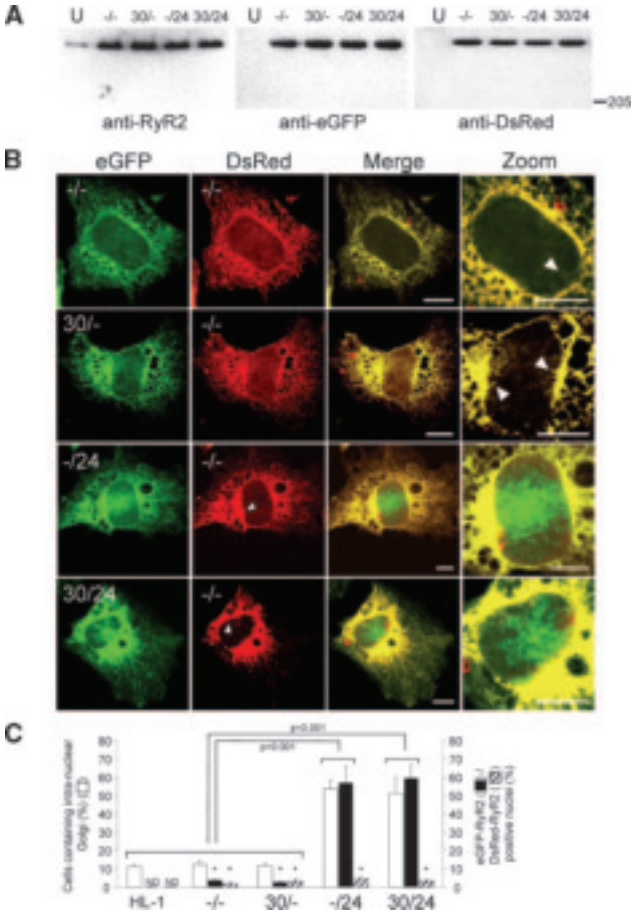

Figure 3. Intranuclear localization of RyR2 requires a 24-bp insertion. A, Cell lysates (200 μg) from HL-1 cardiomyocytes coexpressing eGFP-tagged splice variants and DsRed-tagged $RyR2^{-/-}$ were analyzed by immunoblotting as indicated. B, The intracellular localization of eGFP-tagged variants (green) and DsRed-tagged RyR2 variants (red) were determined. Coincident signals appear yellow (Merge). Arrowheads depict intranuclear structures consistent with NR. Bar represents 10 μm. C, The occurrence of INGA (white bars) and the localization of eGFP-tagged RyR2 splice variants (black bars) and DsRed-tagged $RyR2^{-/-}$ (hatched bars) were quantified. Data are derived from analysis of >120 cells (n=6). *$P<0.005$ within grouping. ND indicates not determined.

pressing different levels of eGFP-tagged RyR2 splice variants showed that the INGA localization of $RyR2^{-/24}$ and $RyR2^{30/24}$ was not an artifact of cellular overexpression (supplemental Figure II). Although $RyR2^{-/-}$ and $RyR2^{30/-}$ were found in the NR invaginations, we did not detect these variants in INGA-like structures, suggesting that the 24-bp insertion was a key determinant of RyR2 localization to this intranuclear compartment.

To further investigate these observations, we used the obligate tetramerization required for DsRed fluorescence.[15] eGFP-tagged RyR2 splice variants and DsRed-tagged $RyR2^{-/-}$ were coexpressed to equivalent levels (Figure 3A). eGFP-tagged $RyR2^{-/-}$ and $RyR2^{30/-}$ extensively colocalized with DsRed-tagged $RyR2^{-/-}$ in the ER network, NR projections, and perinuclear regions (Figure 3B, arrowheads), but we did not detect these variants in INGA. Coexpression of eGFP-tagged $RyR2^{-/24}$ or $RyR2^{30/24}$ with DsRed-tagged $RyR2^{-/-}$ also resulted in significant colocalization in extranuclear and NR compartments (Figure 3B). Importantly, we determined a striking intracellular segregation of RyR2 splice variants, because INGA localization was exclusively restricted to eGFP-tagged $RyR2^{-/24}$ and $RyR2^{30/24}$ and there was a marked absence of homotetrameric DsRed-tagged $RyR2^{-/-}$ in this compartment (Figure 3B and 3C, "green only" intranuclear fluorescence). Moreover, the proportion of INGA-localized eGFP-tagged $RyR2^{-/24}$ and $RyR2^{30/24}$ in these coexpression experiments was similar to those in which these were the only variants expressed ($RyR2^{-/24}$, 11.9±2.8% and $RyR2^{30/24}$, 9.6±3.7% of the total cellular recombinant protein), indicating that coexpression of DsRed-tagged RyR2 did not inhibit the INGA localization of RyR2 containing the 24-bp splice insertion (Figure 3C). These data strongly suggested that although all RyR2 splice variants exhibited limited nuclear localization by virtue of NR invaginations (Figures 2B and 3B), the 24-bp insertion was necessary for RyR2 localization in INGA, thereby conferring subcellular segregation of RyR2 variants.

RyR2 Splice Variants Modulate Cardiomyocyte Ca^{2+} Signaling and Susceptibility to Apoptosis

Using caffeine as a quasiphysiological activator of Ca^{2+}-dependent RyR2 Ca^{2+} release, we investigated the role of differential cellular localization of RyR2 splice variants on cardiomyocyte Ca^{2+} signaling. Cytoplasmic and nuclear Ca^{2+} levels were comparable in nonstimulated cells expressing all RyR2 variants (Figure 4C), but only cells expressing RyR2 containing the 30-bp or 24-bp exons exhibited suppressed cytoplasmic Ca^{2+} transients in response to acute caffeine stimulation (Figure 4B and 4C), possibly reflecting reduced Ca^{2+} release from the ER and the perinuclear GA. In contrast, nuclear Ca^{2+} mobilization (comprising Ca^{2+} release from the NE, NR, and inward diffusion of Ca^{2+} from the cytosol) was markedly augmented only in $RyR2^{-/24}$ and $RyR2^{30/24}$ cells (Figure 4B and 4C). The amplitude of caffeine-evoked cytoplasmic and nuclear Ca^{2+} mobilization was not an index of the cellular Ca^{2+} content because the total cellular Ca^{2+} mobilization in response to thapsigargin-mediated (5μmol/L) ER depletion was equivalent in each cell type ($RyR2^{30/-}$, 104±18%; $RyR2^{-/24}$, 97±11%; and $RyR2^{30/24}$, 93±16%; normalized to $RyR2^{-/-}$, 100%). We did not determine the potential effects of RyR2 splice variant expression on discrete cytoplasmic and nuclear Ca^{2+} storage and/or availability. Consequently, the altered caffeine-induced nuclear and cytoplasmic Ca^{2+} mobilization in cells expressing RyR2 containing 30-bp or 24-bp insertions were probably attributable to factors other than cellular Ca^{2+} content (see Discussion).

Analysis of the temporal aspects of caffeine-evoked Ca^{2+} mobilization revealed that the rate of cytoplasmic Ca^{2+} increase following caffeine addition was comparable in cells expressing all RyR2 variants, although $RyR2^{-/24}$ and $RyR2^{30/24}$ exhibited a significantly faster recovery of resting cytoplasmic Ca^{2+} levels (Figure 4C). In contrast, the augmented nuclear Ca^{2+} transients mediated by $RyR2^{-/24}$ and $RyR2^{30/24}$ (Figure 4B and 4C) exhibited more rapid rise times and recovery to basal levels than cytoplasmic Ca^{2+} transients (Figure 4C).

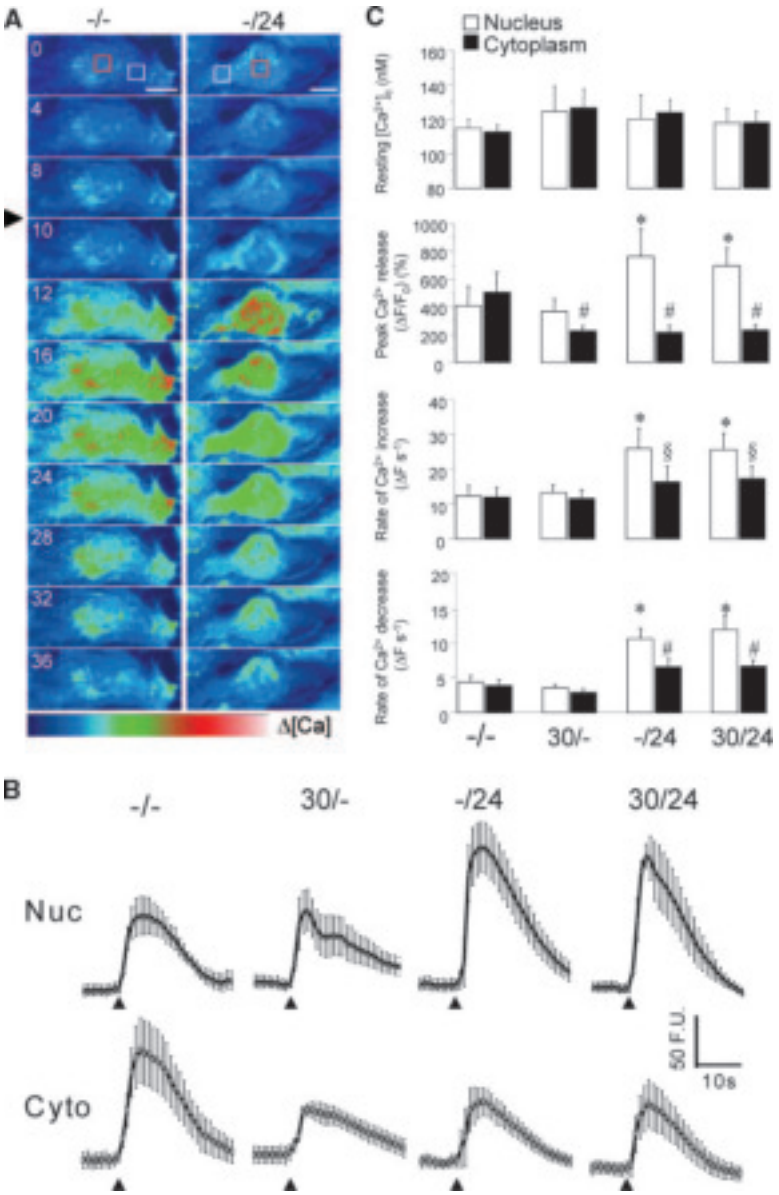

Figure 4. RyR2 splice variants differentially modulate cellular Ca^{2+} release following acute channel activation. A, Pseudocolored images of fluo3-loaded cells expressing RyR2 splice variants before and after the application of a bolus of caffeine (10 mmol/L) (black arrow) at time intervals (seconds) shown. Typical cytoplasmic and nuclear regions analyzed are given in white and red, respectively. Bar represents 10 μm. B, The average profiles of Ca^{2+} mobilization in nuclear and cytoplasmic regions triggered by caffeine addition (10 mmol/L) (arrowhead). Data are given as mean±SEM (n>12 cells in at least 4 experiments). C and D, The amplitude (C) and temporal (D) aspects of nuclear and cytoplasmic Ca^{2+} release were quantified. *P<0.05 when compared with $RyR2^{-/-}$; #P<0.05 when compared within grouping and with $RyR2^{-/-}$; §P<0.05 when compared within grouping.

Normal cardiomyocyte function occurs against a background of large cytoplasmic Ca^{2+} fluctuations, and normal cell phenotype is maintained following acute caffeine-induced Ca^{2+} mobilization.[8] However, small but persistent perturbations in Ca^{2+} homeostasis arising from chronic exposure to caffeine (1 mmol/L) promoted cardiomyocyte dysfunction.[16] Thus, we investigated the functional impact of RyR2 splice variants on cellular Ca^{2+} signaling and phenotype in response to prolonged exposure to caffeine (1 mmol/L). Under nonstimulated conditions, nuclear and cytoplasmic Ca^{2+} amplitude variation (Ca^{2+}"flux") was suppressed in all cells expressing RyR2 containing 30^{+} and 24^{+} insertions when compared with that occurring in cells expressing $RyR2^{-/-}$ (Figure 5A and 5B), indicating that reduced basal Ca^{2+} fluxes were independent of the distinct subcellular localization of $RyR2^{30/-}$, $RyR2^{-/24}$, and $RyR2^{30/24}$ (Figure 2). The reduced Ca^{2+} fluxes were probably caused by altered basal activity of RyR2 splice variants, because a comparable reduction in the magnitude of Ca^{2+} flux through $RyR2^{-/-}$ channels was achieved following ryanodine inhibition (Figure 5A and 5B). However, tonic activation of RyR2 following prolonged caffeine exposure (1 mmol/L, 16 hours), manifested as persistently increased nuclear and cytoplasmic Ca^{2+} fluxes in $RyR2^{-/-}$ and $RyR2^{30/-}$ cells (Figure 5A and 5C). In contrast, caffeine-triggered Ca^{2+} fluxes were significantly reduced in $RyR2^{-/24}$ and $RyR2^{30/24}$ cells (Figure 5A and 5C)

We next investigated the phenotypic consequences of differential suppression of Ca^{2+} fluxes by distinct RyR2 splice variants. The extent of cell death (occurring via necrosis and apoptosis) within HL-1 populations is typically 8% to 10%, and this is not affected by the expression of $RyR2^{-/-}$ or other splice variants (Figure 6A). However, the reduced "resting" nuclear and cytoplasmic Ca^{2+} flux in nonstimulated cardiomyocytes expressing RyR2 contain-

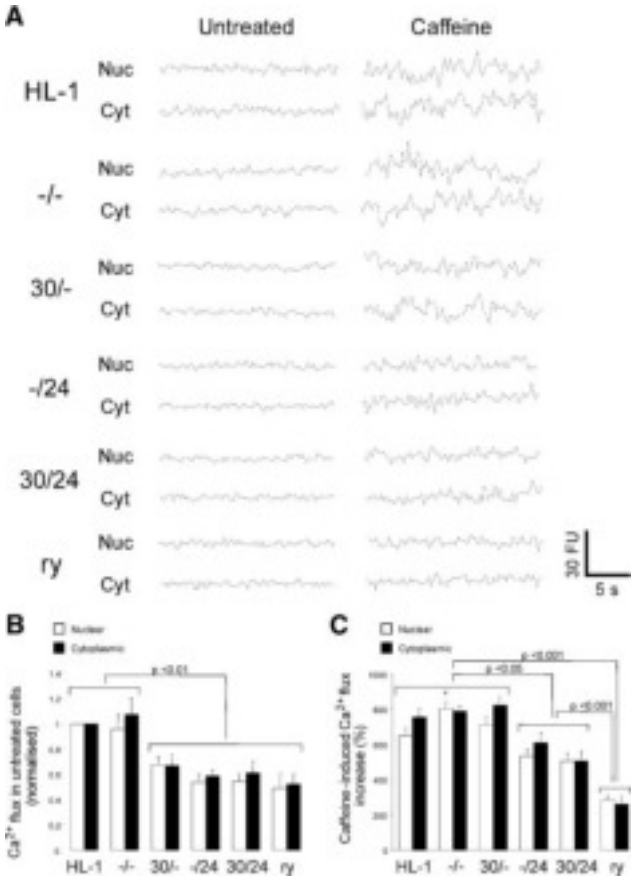

Figure 5. The 24-bp insertion suppresses intracellular Ca^{2+} fluxes during prolonged caffeine exposure. A, Ca^{2+} traces from nuclear and cytoplasmic regions in untreated cells or those exposed to caffeine (1 mmol/L, 16 hours). The effect of ryanodine (1 mmol/L) on $RyR2^{-/-}$ is shown (ry). B, The amplitude and temporal variability ("noise") in Ca^{2+} signal fluxes obtained from nuclear and cytoplasmic regions (white and black bars, respectively) in nonstimulated cells was normalized to the signal variability in nontransfected HL-1 cells (assigned 1).[8,9] C, The increased nuclear and cytoplasmic Ca^{2+} signal variability following prolonged exposure to caffeine (1 mmol/L, 16 hours) was calculated. Data are given as the mean±SEM (n=4 experiments, >20 cells per experiment). *$P<0.05$ when compared with nuclear Ca^{2+} signal variability in HL-1 cells and those expressing $RyR2^{30/-}$.

ing 30-bp or 24-bp insertions was associated with a significant reduction in the basal levels of apoptosis (Figure 6A and 6B). Apoptosis was markedly increased in caffeine-activated cells expressing $RyR2^{-/-}$ (Figure 6A). Notably, although $RyR2^{30/-}$ reduced nuclear and cytoplasmic Ca^{2+} fluxes in nonstimulated cells, and reduced the basal levels of apoptosis (Figure 6A), $RyR2^{30/-}$ did not protect cells from apoptosis following prolonged caffeine exposure (Figure 6A). In contrast, apoptosis was dramatically reduced in cells expressing $RyR2^{-/24}$ and $RyR2^{30/24}$ following caffeine stimulation (Figure 6A). Thus our data reveal a clear link between the magnitude of RyR2-dependent nuclear and cytoplasmic Ca^{2+} fluxes and the extent of apoptosis (Figure 6B), a finding that was reinforced by the pronounced anti-apoptotic effects of channel inhibition using ryanodine (Figures 5C and 6).

These data established a clear functional consequence of 24-bp exon insertion, namely a markedly reduced caffeine-induced Ca^{2+} flux that was innately linked to a reduced apoptotic propensity. Because the Bcl-2 family of proteins have been shown to be involved in the signaling of apoptosis following agonist-triggered RyR2-dependent Ca^{2+} release,[17] we investigated whether the antiapoptotic effects of 24-bp splice insertion following prolonged caffeine exposure was linked to alterations in the expression or posttranslational modification of Bcl-2. We did not detect significant changes in Bcl-2 transcription or in the cellular levels of Bcl-2 protein in cells expressing RyR2 splice variants (Figure 7A and 7B). However, we determined significantly increased levels of Bcl-2 phosphorylation in $RyR2^{-/24}$ and $RyR2^{30/24}$ cells. These data suggest that the protection from apoptosis conferred by expression of RyR2 containing the 24-bp splice insertion may be linked to an alteration in the phosphorylation status of Bcl-2.

RyR2 Alternative Splicing Exhibits Developmental Regulation and Tissue and Species Specificity

We determined the species, tissue, and developmental profile of RyR2 alternative splicing. In human cardiac tissue, we identified pronounced developmental regulation of 30-bp–containing mRNA transcripts, and this insertion was far more abundant in embryonic heart (>90%) than in adult heart tissue, where it accounted for <20% of the total RyR2 (Figure 7A). The disparate relative abundance of the 30-bp insertion in human and mouse embryos strongly indicated a species-dependent regulation of this variant in developing mammalian heart (Figure 7C and 7D). We did not detect the 30-bp insertion in mRNA transcripts derived from adult rat, rabbit, and mouse hearts, and thus the exclusive detection of this variant in adult human heart may represent an intriguing feature of human cardiac regulation (Figure 7D). RyR2 is also the predominant isoform in brain, and, in stark, contrast to its profile in adult heart, the 30-bp insertion was abundant in adult human hippocampus, suggesting that, in humans, alternative splicing of the 30-bp exon exhibits tissue-specific regulation (Figure 7B). In contrast, mRNA transcripts containing the 24-bp splice variant were detected at comparable levels in all species investigated (≈15% to 25% of total RyR2) (Figure 7D), and we found no evidence of its developmental regulation (Figure 7C). Our screening strategy did not resolve the abundance of RyR2 containing both 30-bp and 24-bp insertions ($RyR2^{30/24}$) in mammalian tissues, although our functional characterization suggests that channels formed from $RyR2^{30/24}$ are indistinguishable from those of $RyR2^{-/24}$.

Discussion

We investigated the role of RyR2 splice variants in cardiomyocytes and present the first evidence that developmentally regulated, tissue-specific splice variants of RyR2 have profound effects on organelle structure, Ca^{2+} signaling, and susceptibility to apoptosis. In skeletal myotubes, nuclear Ca^{2+} signaling is shaped via RyR1 localized to NR projections deep into the nucleus,[14] and nuclear and cytoplasmic Ca^{2+} release events in cardiomyocytes are markedly different.[18] We now demonstrate that in HL-1 cardiomyocytes, all RyR2 variants exhibited NR localization, although the 24-bp inser-

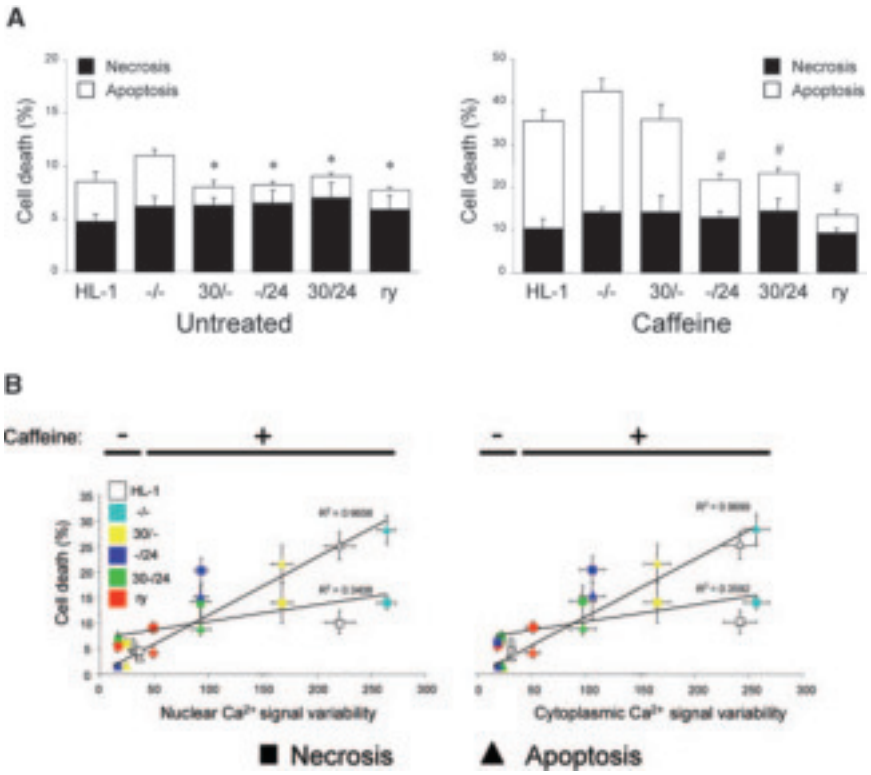

Figure 6. Expression of RyR2 containing the 24-bp splice insertion protects cells from caffeine-induced apoptosis. A, The extent of apoptosis vs necrosis in resting and caffeine-activated cells is shown. *$P<0.05$ and #$P<0.001$, respectively, when compared with nontransfected HL-1 cardiomyocytes. B, The mode of cell death was plotted against the Ca^{2+} signal flux (see Figure 5) in nuclear and cytoplasmic compartments in nonstimulated (−) and caffeine-activated (1 mmol/L, 16 hours) (+) cells expressing RyR2 splice variants (color coded as shown). Data are plotted as the mean±SEM (n=4, >20 cells per experiment), and R^2 values are given. In A and B, the effects of ryanodine inhibition of $RyR2^{-/-}$ is given (ry).

tion was essential for the localization of this RyR2 splice variant to a distinct intranuclear structure that was morphologically identical to an intranuclear GA, presently termed INGA (Figures 2 and 3). Nuclear Golgi "tendrils" have been previously identified in atrial cardiomyocytes[19], and tubular transnuclear structures that modulate intracellular Ca^{2+} signaling have been reported,[20] suggesting that INGA is not an idiosyncratic feature of HL-1 cells (supplemental Figure III). However, our data suggest that currently unknown molecular mechanisms may act as "gate-keepers" to selectively incorporate RyR2 channels containing the 24-bp insertion into this compartment. Consequently, an important conclusion of the present study is that alternative splicing contributes to the intracellular segregation of RyR2 variants. The role of alternative splicing in determining RyR targeting to other cellular compartments including mitochondria,[21] cytoplasmic GA,[22] and plasma membrane[23] is unknown. The protein sequences encoded by the 30- and 24-bp insertions do not represent known organelle targeting motifs, but they do exhibit limited sequence homology with domains present within K^+ channels and ankyrin (Figure IV). The 30-bp insertion deletes a putative protein kinase C phosphorylation site found at 1479Ser-Ile-Lys1481, although the functional significance of this remains to be determined.

The present study provides evidence that RyR2 splice variants fundamentally contribute to shaping nuclear and cytoplasmic events, a significant finding given that spatially distinct Ca^{2+} release events underpin altered gene transcription.[24] Consequently, our data suggest that the precise control of cardiomyocyte Ca^{2+} handling via differential RyR2 splice variant expression may play an important role in modulating diverse aspects of cardiac cell signaling, rather than in simply controlling the mechanics of heart muscle contraction. We do not yet know the precise basis for the differential Ca^{2+} release mediated by the distinct RyR2 splice variants, although we interpret our results to suggest that cell-compartment–specific regulation by currently unknown nuclear and/or cytoplasmic factors (including the relative contribution of ER-, NR-, GA-, and INGA-derived Ca^{2+} sources, the differences in subcellular architecture, and differential nuclear and cytoplasmic protein–protein interactions) may contribute to the distinct Ca^{2+} modulation.

We reveal a strong link between reduced RyR2-dependent Ca^{2+} fluxes following 24-bp insertion and the protection from caffeine-induced apoptosis (Figures 5 and 6). This important finding is entirely consistent with the reduced channel activity determined in some 1,4,5-trisphosphate receptor and RyR3 splice variants,[5,25] although further work is needed to conclusively determine whether the INGA localization of the 24-bp–containing splice variant is a critical determinant of the observed antiapoptotic effects. Importantly, our data show that the suppression of caffeine-evoked Ca^{2+} fluxes mediated by RyR2 containing the 24-bp splice insertion was associated with altered Bcl-2 phosphorylation. This new evidence indicates that the interplay between Ca^{2+} flux, Bcl-2 phosphorylation, and apoptosis can be modulated by the specific expression of distinct RyR2 splice variants. The precise mechanisms through which Bcl-2 family proteins transduce RyR2-dependent Ca^{2+} fluxes in apoptotic signaling remain to be determined, and one should consider that caffeine-evoked apoptosis may be attributable to other mechanisms, in addition to perturbations in Ca^{2+} fluxes,

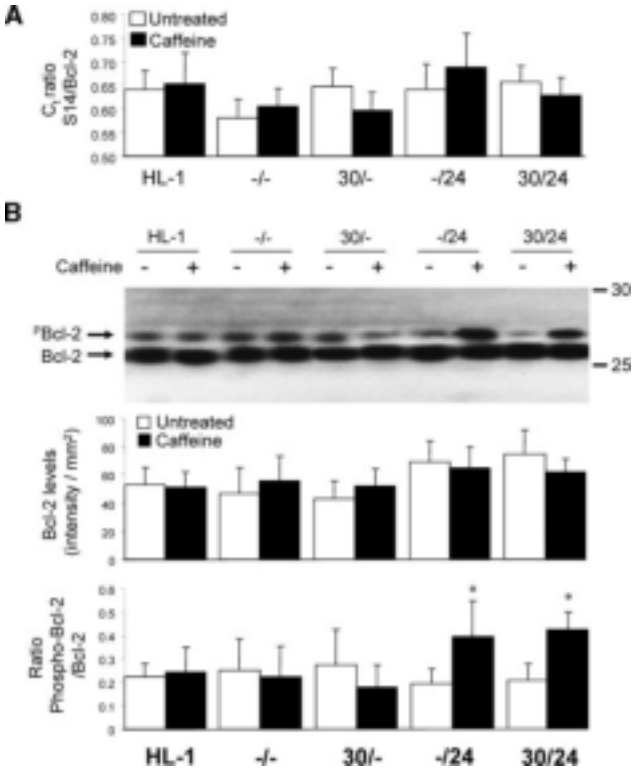

Figure 7. Expression of RyR2 containing the 24-bp splice insert is associated with increased phosphorylation of Bcl-2 following caffeine stimulation. A, The levels of Bcl-2 transcription in untreated cells or those exposed to caffeine (1 mmol/L, 16 hours) was determined using quantitative PCR as described in the online data supplement. The ratios of the threshold crossing point (C_t) of a control transcript, S14 ribosomal protein, to that of Bcl-2 in each instance were calculated (mean±SEM, n=3 cell populations in each instance). B, Immunoblot analysis of Bcl-2 expression in untreated cells or following prolonged exposure to caffeine (1 mmol/L, 16 hours). Phosphorylated Bcl-2 (^{P}Bcl-2) appears as the upper band of the doublet. Data are plotted as means±SEM and are derived from 4 separate blots. *$P<0.05$ when compared within group and when compared with caffeine-treated HL-1 cells or cells expressing $RyR2^{-/-}$ and $RyR2^{30/-}$. Reduced Bcl-2 phosphorylation was consistently observed in $RyR2^{30/-}$ cells following caffeine exposure but did not reach significance when compared with caffeine-treated HL-1 cells ($P=0.14$) and untreated $RyR2^{30/-}$ cells ($P=0.27$).

including the activation of a number of cAMP-dependent pathways.

Although we show that developmentally regulated RyR2 splicing occurs in human heart (Figure 7), the relative abundances of 30-bp and 24-bp insertions identified in embryonic and adult transcripts do not provide an accurate insight into the channel subunit stoichiometry occurring in vivo. The adult human heart is a highly heterogeneous tissue composed of numerous cell types tailored for specialized function. It is possible that the 2 RyR2 splice variants can be coexpressed in the same cells, or differentially distributed in distinct cell types within the myocardium.[26] Furthermore, we do not know the precise stoichiometric arrangement of the RyR2 tetramers generated in our experiments, although the approximate 4-fold overexpression of recombinant RyR2 would predict that most recombinant RyR2 channels exist in homotetrameric combination. Notably, the 24-bp insertion appeared to be "dominant," because the functional characteristics of RyR2 containing both 24- and 30-bp splice insertions were indistinguishable from RyR2 containing only the 24-bp insertion.

The Therapeutic Potential of Manipulating Cardiac Phenotype by Alternative Splicing

During development, cell-specific regulatory pathways dictate the intrinsic susceptibility of the cells to die. Embryonic human hearts were characterized by very high levels of 30-bp–containing transcripts, splice variants that do not protect cells from increased Ca^{2+} fluxes and apoptosis. The abundance of this variant in embryonic heart (Figure 8) may limit the incorporation of antiapoptotic RyR2 containing the 24-bp insertion into functional tetramers, and we speculate that the high levels of RyR2 containing the 30-bp splice insertion may indirectly confer apoptotic susceptibility during cardiac development. Apoptosis is a critical determinant of embryonic myocardial architecture, but it may also be important in normal adult heart remodeling.[27] The long-term adaptive value of apoptosis in the adult myocardium, and its place as a target for therapeutic intervention, remains to be determined. The adult heart can be repaired by gene-based reprogramming of embryonic signaling patterns,[28] and thus our demonstration that cardiomyocyte Ca^{2+} signaling and phenotype can be fine-tuned by the expression of functionally distinct RyR2 splice variants potentially represents a novel approach to future cardiac therapies.

Limitations of Study

We have not succeeded in generating antibodies that specifically recognize the distinct RyR2 splice variants, and it is not currently possible to investigate the developmental profiles and intracellular localization of these variants in native cardiac tissue, or primary cell cultures at the protein level. Accordingly, at the present time, a functional characterization of RyR2 splice variants is restricted to heterologous expression systems. Despite this, HL-1 cardiomyocytes retain the contractile and phenotypic properties of adult cardiomyocytes[29] and express recombinant RyR2 that, in our hands, is indistinguishable from the endogenous protein.[8,9] Thus HL-1 cells represent the best heterologous system currently available for evaluating the role of RyR2 splice variants in cardiomyocyte Ca^{2+} signaling. Analysis of HL-1–derived mRNA transcripts (at passage nos. 37, 55, and 87) showed that endogenous RyR2 lacked the 30- and 24-bp insertions (0/18 and 0/25 transcripts, respectively), and although this is entirely consistent with the progressive loss of RyR1 splice insertions during skeletal myotube culture,[4] HL-1 cells may not reflect the RyR2 splicing events that occur in the myocardium in vivo.

Sources of Funding

This work was supported by the British Heart Foundation (FS/2000020, BS/04/002, PG/98169), the Royal Society (2004/R2), the Medical Research Council, and the European Union (LSHM-CT-2005-018802).

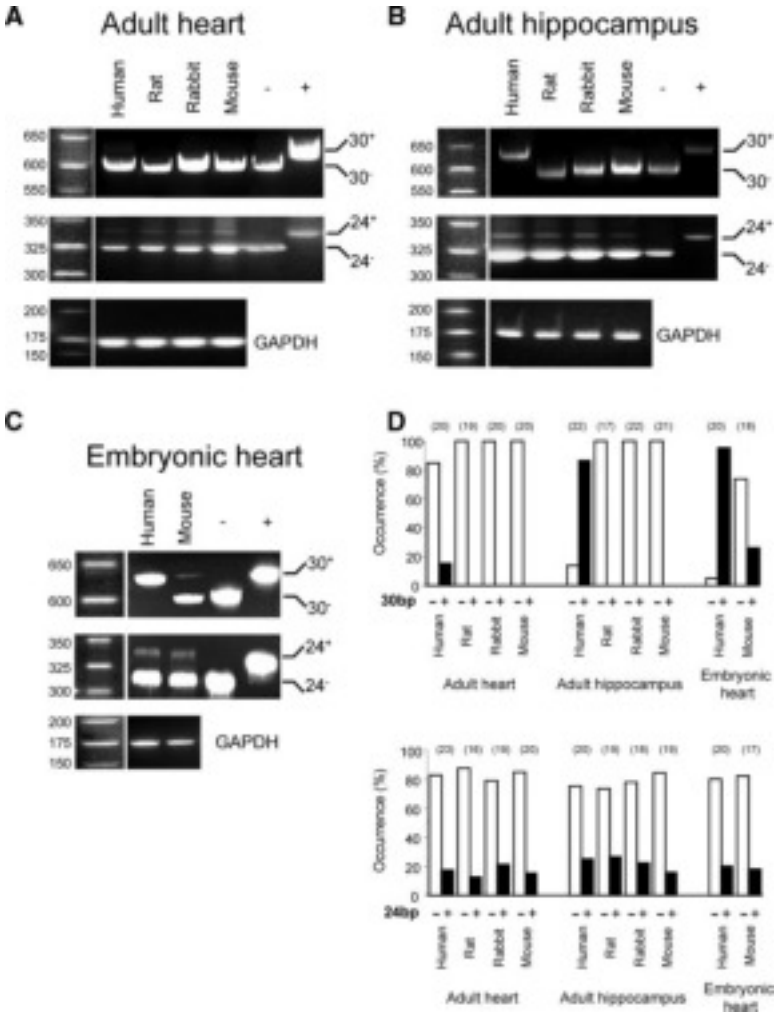

Figure 8. Developmental regulation and tissue specificity of RyR2 alternative splicing. RyR2 alternative splicing in adult heart (A), adult hippocampus (B), and embryonic heart (C) from various species was determined. Recombinant RyR2 fragments with or without splice insertions (+ and −, respectively) were used as controls. Amplification of glyceraldehyde-3-phosphate dehydrogenase (GAPDH) transcripts was used to verify equivalent amounts of cDNA templates. D, The presence (+, black bars) or absence (-, white bars) of 30- and 24-bp insertions in PCR-amplified fragments. The number of fragments analyzed by DNA sequencing is given in parentheses.

Disclosures

None.

References

1. Fill M, Copello JA. Ryanodine receptor calcium release channels. *Physiol Rev*. 2002;82:893–922.
2. Meissner G. Molecular regulation of cardiac ryanodine receptor ion channel. *Cell Calcium*. 2004;35:621–628.
3. George CH, Yin CC, Lai FA. Toward a molecular understanding of the structure:function of ryanodine receptor Ca^{2+} release channels: perspectives from recombinant expression systems. *Cell Biochem Biophys*. 2005;42:197–222.
4. Kimura T, Nakamori M, Lueck JD, Pouliquin P, Aoike F, Fujimura H, Dirksen RT, Takahashi MP, Dulhunty AF, Sakoda S. Altered mRNA splicing of the skeletal muscle ryanodine receptor and sarcoplasmic/endoplasmic reticulum Ca^{2+}-ATPase in myotonic dystrophy type 1. *Hum Mol Genet*. 2005;14:2189–2200.
5. Jiang D, Xiao B, Li X, Chen SRW. Smooth muscle tissues express a major dominant negative splice variant of the type 3 Ca^{2+} release channel (ryanodine receptor). *J Biol Chem*. 2003;278:4763–4769.
6. Dabertrand F, Morel JL, Sorrentino V, Mironneau J, Mironneau C, Macrez N. Modulation of calcium signalling by dominant negative splice variant of ryanodine receptor subtype 3 in native smooth muscle cells. *Cell Calcium*. 2006;40:11–21.
7. Tunwell REA, Wickenden C, Bertrand BMA, Shevchenko VI, Walsh MB, Allen PD, Lai FA. The human cardiac muscle ryanodine receptor-calcium release channel: identification, primary structure and topological analysis. *Biochem J*. 1996;318:477–487.
8. George CH, Higgs GV, Lai FA. Ryanodine receptor mutations associated with stress-induced ventricular tachycardia mediate increased calcium release in stimulated cardiomyocytes. *Circ Res*. 2003;93:531–540.
9. George CH, Jundi H, Thomas NL, Walters N, West RR, Lai FA. Arrhythmogenic mutation-linked defects in ryanodine receptor autoregulation reveal a novel mechanism of Ca^{2+} release channel dysfunction. *Circ Res*. 2006;98:88–97.
10. George CH, Jundi H, Thomas NL, Scoote M, Walters N, Williams AJ, Lai FA. Ryanodine receptor regulation by intramolecular interaction between cytoplasmic and transmembrane domains. *Mol Biol Cell*. 2004;15:2627–2638.
11. George CH, Higgs GV, Mackrill JJ, Lai FA. Dysregulated ryanodine receptors mediate cellular toxicity: restoration of normal phenotype by FKBP12.6. *J Biol Chem*. 2003;278:28856–28864.
12. Leist M, Jaattela M. Four deaths and a funeral: from caspases to alternative mechanisms. *Nat Rev Mol Cell Biol*. 2001;2:589–598.
13. Echevarria W, Leite MF, Guerra MT, Zipfel WR, Nathanson MH. Regulation of calcium signals in the nucleus by a nucleoplasmic reticulum. *Nat Cell Biol*. 2003;5:440–446.
14. Marius P, Guerra MT, Nathanson MH, Ehrlich BE, Leite MF. Calcium release from ryanodine receptors in the nucleoplasmic reticulum. *Cell Calcium*. 2006;39:65–73.
15. Baird GS, Zacharias DA, Tsien RY. Biochemistry, mutagenesis, and oligomerization of dsRed, a red fluorescent protein from coral. *Proc Natl Acad Sci U S A*. 2000;97:11984–11989.
16. Balasubramaniam R, Chawla S, Grace AA, Huang CL-H. Caffeine induced arrhythmias in murine hearts parallel changes in cellular Ca^{2+} homeostasis. *Am J Physiol Heart Circ Physiol*. 2005;289:H1584–H1593.
17. Pan Z, Damron D, Nieminen AL, Bhat MB, Ma J. Depletion of intracellular Ca^{2+} by caffeine and ryanodine induces apoptosis of Chinese hamster ovary cells transfected with ryanodine receptor. *J Biol Chem*. 2000;275:19978–19984.
18. Yang Z, Steele DS. Characteristics of prolonged Ca^{2+} release events associated with the nuclei in adult cardiac myocytes. *Circ Res*. 2005;96:82–90.

19. Rambourg A, Segretain D, Clermont Y. Tridimensional architecture of the Golgi apparatus in the atrial muscle cell of the rat. *Am J Anat*. 1984;170:163–179.
20. Lui PPY, Chan FL, Suen YK, Kwok TT, Kong SK. The nucleus of HeLa cells contains tubular structures for Ca^{2+} signalling with the involvement of mitochondria. *Biochem Biophys Res Commun*. 2003;308:826–833.
21. Beutner G, Sharma VK, Giovannucci DR, Yule DI, Sheu SS. Identification of ryanodine receptor in rat heart mitochondria. *J Biol Chem*. 2001;276:21482–21488.
22. Cifuentes F, Gonzalez CE, Fiordelisio T, Guerrero G, Lai FA, Hernandez-Cruz A. A ryanodine fluorescent derivative reveals the presence of high-affinity ryanodine binding sites in the Golgi complex of rat sympathetic neurons, with possible functional roles in intracellular Ca^{2+} signalling. *Cell Signal*. 2001;13:353–362.
23. Zaidi M, Shankar VS, Tunwell R, Adebanjo OA, Mackrill J, Pazianas M, O'Connell D, Simon BJ, Rifkin BR, Venkitaraman AR, Huang CL-H, Lai FA. A ryanodine receptor-like molecule expressed in the osteoclast plasma membrane functions in extracellular Ca^{2+} sensing *J Clin Invest*. 1995;96:1582–1590.
24. Hardingham GE, Chawla S, Johnson CM, Bading H. Distinct functions of nuclear and cytoplasmic calcium in the control of gene expression. *Nature*. 1997;385:260–265.
25. Iwai M, Tateishi H, Hattori M, Mizutani A, Nakamura T, Futatsugi A, Inoue T, Furuichi T, Michikawa T, Mikoshiba K. Molecular cloning of mouse type 2 and type 3 inositol 1,4,5-trisphosphate receptors and identification of a novel type 2 receptor splice variant. *J Biol Chem*. 2005;280:10305–10317.
26. Borgatta L, Watras J, Katz AM, Ehrlich BE. Regional differences in calcium-release channels from heart. *Proc Natl Acad Sci U S A*. 1991;88:2486–2489.
27. Kajstura J, Bolli R, Sonnenblick EH, Anversa P, Leri A. Cause of death: suicide. *J Mol Cell Cardiol*. 2006;40:425–437.
28. Kusano KF, Pola R, Murayama T, Curry C, Kawamoto A, Iwakura A, Shintani S, Ii M, Asai J, Tkebuchava T, Thorne T, Takenaka H, Aikawa R, Goukassian D, von Samson P, Hamada H, Yoon YS, Silver M, Eaton E, Ma H, Heyd L, Kearney M, Munger W, Porter JA, Kishore R, Losordo RW. Sonic hedgehog myocardial gene transfer therapy: tissue repair through transient reconstitution of embryonic signaling. *Nat Med*. 2005;11:1197–1204.
29. Claycomb WC, Lanson NA, Stallworth BS, Egeland DB, Delcarpio JB, Bahinski A, Izzo NJ. HL-1 cells: a cardiac muscle cell line that contracts and retains phenotypic characteristics of the adult cardiomyocyte. *Proc Natl Acad Sci U S A*. 1998;95:2979–2984.

Supplementary methods.

Construction of recombinant RyR2 containing 30bp and 24bp splice insertions.

RyR2$^{-/+}$ was generated by transferring an *NheI-NdeI* fragment (9894-11858bp) from a pBluescript-cloned fragment containing the 24^{+} splice variant (HC7: 9441-11940bp) [1] into full-length RyR2$^{-/-}$ in pcDNA3 [2]. A subsequent in-frame insertion of a PCR-amplified cDNA cassette containing the cytomegalovirus (CMV) promoter proximal to the enhanced green fluorescent protein (eGFP) at *MluI-SpeI* sites placed eGFP four amino acids upstream of the initiating methionine of RyR2$^{-/24}$ [3].

In the absence of any usable restriction sites in the vicinity of the 30bp splice insertion in the original 30^{+}-containing clone (HC2: 4097-5550bp) [1], two fragments encompassing 3801-4437bp **(I)** and 4429-5432bp **(II)** were amplified from full-length RyR2 and HC2, respectively using Pfu polymerase (Promega) and oligonucleotide pairs:

I: BstEII-F, 5' TATAGA**GGTGACC**AGAATAGACGG 3' / I-30^{+}R, 5' CTGGGTCCCGGATATA*AAGCTT*TCATGCACTTTTCC 3'
II: II-30^{+}F, 5' CATGA*AAGCTT*TGCCATTGACT 3' / SanDI-R, 5' CCAACTGGGTCCCGGGCATG 3'
where restriction enzyme sites are shown in **bold** (**BstEII**), underlined (SanDI) and *italics* (*HindIII*).

Blunt-ended PCR products were cloned into the shuttle vector pSL1180 (GE Healthcare) containing a mutant-ablated endogenous *HindIII* site, at a blunt-ended *EcoRV* site. The I-30^{+}R primer introduced *HindIII* and *SanDI* sites at the 3' end of fragment I, and *HindIII/SanDI* digested recombinant plasmid cDNA was ligated with the *HindIII/SanDI* digested fragment II to create an RyR2 cassette containing the 30^{+} (3801-5432bp (30^{+})). The *BstEII/SanDI* fragment (3807-5421 (30^{+})) was transferred into an *AseI*-generated RyR2 fragment (2309-8266bp) in pSL1180, and a subsequent *EcoRV* fragment (3894-6892 (30^{+})) was inserted into *EcoRV* digested eGFP-tagged RyR2$^{-/-}$ and RyR2$^{-/24}$ to generate RyR2$^{30/-}$ and RyR2$^{30/24}$, respectively. All sequences and construct boundaries were verified by automated sequencing (ABI 3700, Applied Biosystems).

Antibodies

Monoclonal antibodies against eGFP (clone JL-8) (Clontech) and DsRed (Clontech) were used for immunoblotting as described elsewhere [3, 4]. A rabbit polyclonal antibody raised against calreticulin [5] and a goat polyclonal raised against a Golgi-matrix 130 kDa protein (GM130) (Santa Cruz Biotechnology) were used to determine the intracellular distribution of the endoplasmic reticulum (ER) and Golgi apparatus (GA), respectively . Secondary detection was performed using Alexa-conjugated antibodies (Molecular Probes) and detailed protocols have been described previously [2, 3, 6].

Assessing the intracellular localisation of RyR2 splice variants.

Fluorescent images from antibody labelling (endogenous proteins) or eGFP/DsRed (recombinant RyR2) were acquired using confocal microscopy (RS2, Leica Microsystems) at 1024 x 1024 pixels using 4x line averaging. None of the images contained saturated pixels and thus all fluorescence data was within the linear range. Cell boundaries were defined using Leica Confocal Software (LCS) and total cellular fluorescence from either red or green channels was quantified. Likewise, the nucleus was identified and 'nuclear' fluorescent signals (corresponding to both NR and INGA) were determined, as were those specifically attributable to NR (finger-like invaginations (see Figure 1S), or INGA (tendril-like structures connecting the nuclear poles, see Figure 2B, RyR2$^{-/24}$ and $^{30/24}$). The proportion of total cellular fluorescence due to eGFP or DsRed that localised to these cellular compartments was determined. For all compartments, signal thresholding was used to identify fluorescent pixels > 1.2 times the intensity of average background signals (LCS software).

Ca^{2+} imaging and signal noise analysis

All Ca^{2+} imaging was performed using a confocal microscope (RS2, Leica Microsystems) equipped with a 63x oil-immersion objective (1.32NA), a pinhole diameter set at 1 Airy unit and a refractive index of 1.518. These parameters give an optical z-thickness (i.e. confocality) of ~770nm, and thus there is negligible bleed through of Ca^{2+}-dependent fluorescence from 'out-of-focus' events in the z-axis. Cytoplasmic and nuclear regions analysed were typically separated by >4μm thereby minimising inter-compartmental signal bleed through in the x and y axes (see Figure 4A, white and red boxes).

Ca^{2+}-dependent fluo-3 signals (F) were converted to cytoplasmic Ca^{2+} concentrations ($[Ca^{2+}]_c$) using the equation $[Ca^{2+}]_c = K_{d,app}\ (F-F_{min})/(F_{max}-F)$, where minimum ($F_{min}$) and maximum ($F_{max}$) fluorescence levels were determined following the addition of EGTA (5 mmol/L) and ionomycin (1 μmol/L), respectively and at the end of experiments. The apparent K_d ($K_{d,app}$) of fluo-3 in streptolysin-O permeabilised cells incubated in solutions containing known Ca^{2+} (nominal free Ca^{2+} to 39 μmol/L) was calculated as 631 μmol/L [7].

The amplitude variability (signal noise) between steady-state Ca^{2+} signals obtained from distinct cell populations was determined using the F-ratio as described in detail elsewhere [7]; and the Data Supplement of [4]. The F-ratio is defined as $\boldsymbol{\delta_{HL\text{-}1} / \delta_{RyR2}}$ i.e. the ratio of the variance in Ca^{2+} fluorescent signals in HL-1 cells ($\delta_{HL\text{-}1}$) to those measured in cell populations expressing WT RyR2 or the alternatively spliced variants (δ_{RyR2}). Data was acquired every 200ms and analysed from at least 120 cells from 4 separate experiments in each instance. In Figure 4B, data is plotted as the 1s average of 5 data points (i.e. 5 x 200ms) to simplify data presentation. All other data in Figure 4 is calculated from the raw data acquired at 5Hz.

Transcriptional and protein expression analysis of Bcl-2

Total RNA was extracted from untreated or caffeine-exposed (16h, 1 mmol/L) HL-1 cells or FACS cell populations expressing RyR2 variants -/-, 30/-, -/24 and 30/24 using the RNeasy system (Qiagen). First-strand cDNA was synthesised from total RNA (1µg) using OmniScript reverse transcriptase (Qiagen) and random decamers (10 µmol/L; Ambion) for 90 mins at 37°C. Subsequently, real-time PCR was performed using oligonucleotide pairs (50 nmol/L) specific to Bcl-2 (5'-CCTGTGGATGACTGAGTACC-3' (sense) and 5'-GAGACAGCCAGGAGAAAT-3' (antisense)), or the ribosomal S14 protein ('housekeeping gene') (5'-GGCAGACCGAGATGAACTCT-3' (forward) and 5'-CCAGGTCCAGGGGTCTTGGT-3' (reverse)) in FastStart SYBR Green I DNA reaction mixes (Roche Diagnostics) containing 100ng cDNA template and 4.0 mmol/L $MgCl_2$. Each reaction was cycled using the following parameters: initial denaturation (10min, 95^{o}C) followed by 40 cycles of denaturation (10 sec, 95^{o}C), annealing (5 sec, 60^{o}C) and extension (20 sec, 72^{o}C). Quantitative analysis was performed using LightCycler software version 3.5 (Roche Diagnostics), with real-time fluorogenic detection. To confirm amplification specificity the PCR products were subjected to melting curve analysis. The ratio of Bcl-2:S14 transcripts were calculated from the crossing points of each gene (C_t). The determination of normalised Bcl-2 transcript levels was performed in triplicate using total RNA extracted from separate cell populations in each instance.

The cellular expression levels of Bcl-2 protein was determined by denaturing SDS-PAGE separation of total cellular protein (50µg) on 20% (v/v) polyacrylamide gels followed by immunoblotting using a monoclonal hamster antibody raised against mouse Bcl-2 (clone 3F11, 5µg/ml; BD Pharmingen) and subsequent visualisation using goat anti-hamster HRP-linked secondary antibody (1:7000 dilution; Santa Cruz Biotechnology) and chemiluminescent detection (Supersignal, Pierce) as described previously [2, 3, 6]. Densitometric analysis of immunoblots was performed using a G700 scanner and Quantity One software (Biorad).

Analysis of RyR2 30$^+$ and 24$^+$ splice variants in tissue-derived cDNA.

Adult human heart and embryonic mouse heart (embryonic day 10) cDNA libraries were from Stratagene, and a cDNA library generated from day 53 post-coitum human embryonic heart was obtained from American Type Culture Collection. All other cDNAs were reverse-transcribed from mRNA isolated from fresh tissues (FastTrack™, Invitrogen), using random-primed synthesis of first-strand cDNA (SuperScript™, Invitrogen). All tissues were obtained following full ethical approval and in strict accordance with Institutional and National guidelines. cDNAs were analysed for the presence or absence of the 30bp and 24bp exons using PCR amplification and oligonucleotide primers:

30F: 5' CCACAAAGATTATGCCCAGG 3' / **30R**: 5' CTCTTGAATAATCCCGCC 3', (amplifying a human RyR2 fragment (4116-4718) of 603bp (30^-) and 633bp (30^+), and sequence variation in mouse and rabbit RyR2 results in smaller fragments of 600 and 630bp, respectively) and **24F**: 5' AAGGCACTAAGAGAGTTGAT 3' / **24R**: 5' AAGTTTCAGAGTAGCTGCTA 3' (amplifying a fragment (10967-11283bp) of 317bp (24^-) or 341bp (24^+)). Oligonucleotides corresponding to human (shown above), mouse and rabbit sequences were used for screening respective cDNAs. Rat cDNA templates were screened using human oligonucleotides at lower annealing temperatures. Equivalent regions from RyR2 templates with and without the 30bp exon (HC1 (30^-) and HC2 (30^+)) and the 24bp exon (HC10 (24^-) and HC7 (24^+)) [1] were amplified as controls. The amplification of a 175bp fragment from the 'house-keeping' glyceraldehyde-3-phosphate dehydrogenase (GAPDH) gene (using pan-species primers GAPDH-F: 5' CAACTACATGGTTTACATGTTC 3' / GAPDH-R: 5' GGACTCCACGACGTACTCAGC 3') was used to verify equivalent amounts of cDNA templates per amplification. The relative abundances of the 30bp and 24bp variants were determined by automated DNA sequencing of pTOPOII-cloned PCR products using oligonucleotides primers 30F and 24F (Applied Biosystems 3700).

Splice variant	RyR isoform	Species	Sequence	Reference
a	Drosophila	*Drosophila*	YIPSAGA	8
b	RyR1	Human	AGDIQ	9
		Rabbit	AGDAQ	10, 11
		Mouse	AGDVQ	12
b'	RyR3	Mink	AMQVK	13
		Rabbit	AMQVK	14
c	RyR1	Human	VINRQN	9
		Mouse	VINRQN	12
d	RyR2	Rabbit	VTGSQRSK	15, 16
		Dog	VTGSQRSK	-
d'	RyR2	Human	VTGSQRSK	1
e	RyR3	Rabbit	Δ2359-2575 (frameshift)	14
f	RyR3	Rabbit	+ 3bp @ 6812 intronic	14
g	RyR3	Rabbit	Δ8714-8763 (frameshift)	14
h	RyR3	Mink	Duplicate exons with 64% homology	13
i	RyR3	Mink	LIVRER	13
		Rabbit	LIVRER	14
j	RyR3	Human	Δ11569-11650 (frameshift)	17
k	RyR3	Rabbit	29 amino acids	14
l	RyR3	Mouse	Intron not removed at 11569 (frameshift)	18
m	RyR3	Rabbit	51 amino acids	14
n	RyR2	Human	FAIDSLCGFG	1

Supplementary Table.

Table 1S.

Splice variants ***a-n*** refer to Figure 1A. The splice variant identified in the dog RyR2 sequence can be found via GenBank accession number XM_536330.2

Supplementary Figures.

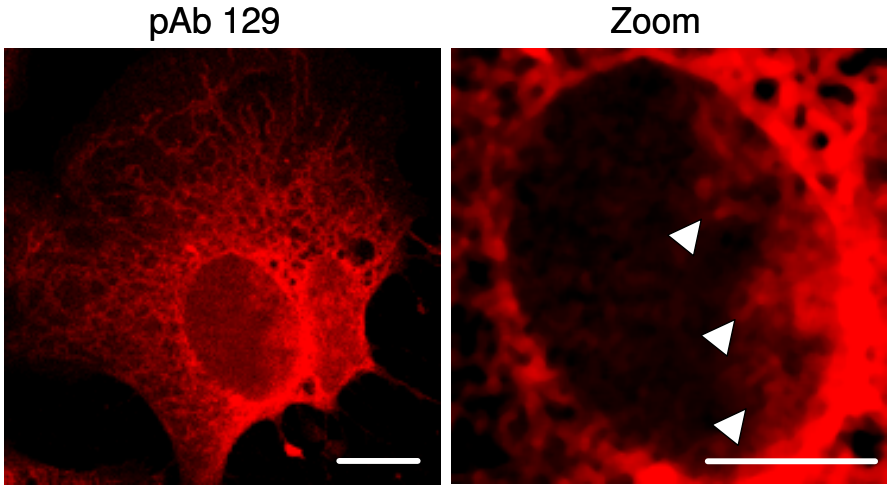

Figure 1S. Endogenous RyR2 in untransfected HL-1 cells was visualised using RyR2 specific antiserum (pAb129) followed by detection using an Alexa-546 conjugated secondary antibody (Molecular Probes). The nuclear region was magnified to show the NR in more detail (arrowed). Bar represents 10μm.

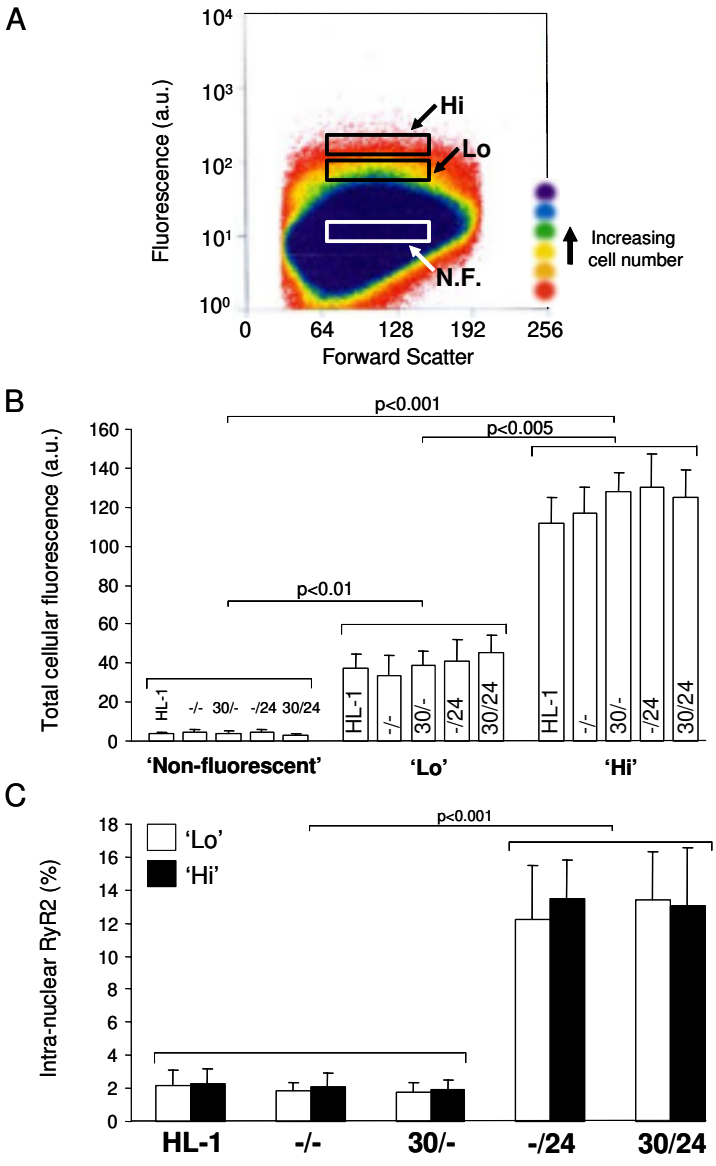

Figure 2S.
(A) HL-1 cells expressing eGFP-tagged RyR2 variants were selected on the basis of cellular fluorescence using FACS as described [4]. Discrete cell populations that expressed high ('Hi') or lower levels ('Lo') of recombinant fluorescent protein, where fluorescence was typically >10-fold and 4-6-fold higher, respectively, than cells that were deemed non-fluorescent (NF) were isolated.
(B) Total cellular fluorescence was determined from single cell analysis of each 'Hi', 'Lo' and 'NF' population using confocal microscopy with constant settings (photomultiplier voltage fixed at 700V, offset voltage fixed at -1.0V, Argon laser set at 25% power) (RS2, Leica Microsystems) and fluorescence was quantified using Leica Confocal Software. Data was obtained from >40 cells in four separate sorts per cell type, and is given as mean values ± SEM. Significance levels between Hi, Lo and NF cell populations are shown, but there were no significant differences within each group.
(C) The proportion of total cellular RyR2 that was localised to intra-nuclear compartments (comprising RyR2 contained in both NR and intra-nuclear Golgi) in 'Lo' and 'Hi' cell populations was determined as described in the Supplementary Methods.

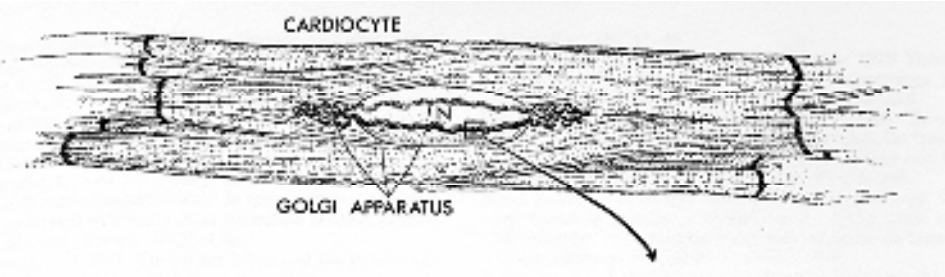

Figure 3S. Nuclear Golgi 'tendrils' that connect the peri-nuclear accumulation of GA at the nuclear poles have been identified in atrial myocytes for over two decades [19]. The cartoon is reproduced with kind permission.

30⁺ splice variant

RyR2 (X98330):	1477	H	E	S	F	A	I	D	S	L	C	G	F	G	I	K	1491
Ether-a-go-go (Q02280):	602	G	E	S	–	–	I	D	S	L	C	F	I	V	T	G	614
Ankyrin (ZP00422043):	141	P	I	S	F	A	I	D	A	L	L	V	Y	V	I	V	155

24⁺ splice variant

RyR2 (X98330):	3713	S	F	E	V	T	G	S	Q	R	S	K	E	K	3725
K^+ channel (XP602167):	758	A	L	K	D	W	G	K	Q	R	S	K	E	R	770

Key:

Identical residues

Hydrophobic residues (hydrophobicity > 0.5 (Black and Mould, 1991))

Figure 4S. Sequence homology of RyR2 splice insertions

References.

1. Tunwell REA, Wickenden C, Bertrand BMA, Shevchenko VI, Walsh MB, Allen PD, Lai FA. The human cardiac muscle ryanodine receptor-calcium release channel: identification, primary structure and topological analysis. *Biochem J.* 1996;318:477-487.
2. George CH, Sorathia R, Bertrand BMA, Lai FA. In situ modulation of the human cardiac ryanodine receptor (hRyR2) by FKBP12.6. *Biochem J.* 2003;370:579-589.
3. George CH, Higgs GV, Lai FA. Ryanodine receptor mutations associated with stress-induced ventricular tachycardia mediate increased calcium release in stimulated cardiomyocytes. *Circ Res.* 2003;93:531-540.
4. George CH, Jundi H, Thomas NL, Walters N, West RR, Lai FA. Arrhythmogenic mutation-linked defects in ryanodine receptor autoregulation reveal a novel mechanism of Ca^{2+} release channel dysfunction. *Circ Res.* 2006;98:88-97.
5. Roderick HL, Campbell AK, Llewellyn DH. Nuclear localisation of calreticulin in vivo is enhanced by its interaction with glucocorticoid receptors. *FEBS Letts.* 1997;405:181-185.

6. George CH, Jundi H, Thomas NL, Scoote M, Walters N, Williams AJ, Lai FA. Ryanodine receptor regulation by intramolecular interaction between cytoplasmic and transmembrane domains. *Mol Biol Cell.* 2004;15:2627-2638.
7. George CH, Higgs GV, Mackrill JJ, Lai FA. Dysregulated ryanodine receptors mediate cellular toxicity: restoration of normal phenotype by FKBP12.6. *J Biol Chem.* 2003;278:28856-28864.
8. Xu X, Bhat MB, Nishi M, Takeshima H, Ma J. Molecular cloning of cDNA encoding a Drosophila ryanodine receptor and functional studies of the carboxyl terminal calcium release channel. *Biophys J.* 2000;78:1270-1281.
9. Zhang Y, Chen HS, Khanna VK, De Leon S, Phillips MS, Schappert K, Britt BA, Brownell KW, MacLennan DH. A mutation in the human ryanodine receptor gene associated with central core disease. *Nat Genet.* 1993;5:46-49.
10. Takeshima H, Nishimura S, Matsumoto T, Ishida H, Kangawa K, Minamino N, Matsuo H, Ueda M, Hanaoka M, Hirose T, Numa S. Primary structure and expression from complementary-DNA of skeletal- muscle ryanodine receptor. *Nature.* 1989;339:439-445.
11. Zorzato F, Sacchetto R, Margreth A. Identification of two ryanodine-receptor transcripts in neonatal, slow-, and fast-twitch skeletal muscles. *Biochem Biophys Res Commun*. 1994;203:1725-1730.
12. Futatsugi A, Kuwajima G, Mikoshiba K. Tissue-specific and developmentally regulated alternative splicing in mouse skeletal muscle ryanodine receptor mRNA. *Biochem J.* 1995;305:373-378.
13. Marziali G, Rossi D, Giannini G, Charlesworth A, Sorrentino V. cDNA cloning reveals a tissue specific expression of alternatively spliced transcripts of the ryanodine receptor type 3 (RyR3) calcium release channel. *FEBS Letts.* 1996;394:76-82.
14. Jiang D, Xiao B, Li X, Chen SRW. Smooth muscle tissues express a major dominant negative splice variant of the type 3 Ca^{2+} release channel (ryanodine receptor). *J Biol Chem.* 2003;278:4763-4769.
15. Nakai J, Imagawa T, Hakamat Y, Shigekawa M, Takeshima H, Numa S. Primary structure and functional expression from cDNA of the cardiac ryanodine receptor/calcium release channel. *FEBS Letts.* 1990;271:169-177.
16. Otsu K, Willard HF, Khanna VK, Zorzato F, Green NM, MacLennan DH. Molecular-cloning of cDNA-encoding the Ca^{2+} release channel (ryanodine receptor) of rabbit cardiac-muscle sarcoplasmic-reticulum. *J Biol Chem.* 1990;265:13472-13483.
17. Leeb T, Brenig B. cDNA cloning and sequencing of the human ryanodine receptor type 3 (RyR3) reveals a novel alternative splice site in the RyR3 gene. *FEBS Letts.* 1998;423:367-370.
18. Miyatake R, Furukawa A, Matsushita M, Iwahashi K, Nakamura K, Ichikawa Y, Suwaki H. Tissue-specific alternative splicing of mouse brain type ryanodine receptor/calcium release channel mRNA. *FEBS Letts.* 1996;395:123-126.
19. Rambourg A, Segretain D, Clermont Y. Tridimensional architecture of the Golgi apparatus in the atrial muscle cell of the rat. *Am J Anat.* 1984;170:163-179.